Simulation of two-step redox recycling of non-stoichiometric ceria with thermochemical dissociation of CO_2/H_2O in moving bed reactors - Part I: Model development with redox kinetics and sensitivity analysis

Azharuddin Farooqui, A. Bose, J. Llorca, M. Santarelli

Abstract

Chemical looping syngas production is a two-step process that produces CO and H_2 from water and CO_2 splitting. This is performed by exploiting a metal oxide as oxygen carrier material, which is thermally reduced and releases oxygen in a subsequent step. The core-process layout is composed of two reactors (oxidation reaction and reduction reactor) and oxygen carriers (metal oxides) circulating between the two reactors. A comprehensive moving-bed reactor model is developed and applied to simulate both the syngas production from water and carbon dioxide by ceria oxidation as well as the thermal reduction of metal oxide. An extensive FORTRAN model is developed to appropriately simulate the complexities of ceria reaction kinetics and implemented as subroutine into an ASPEN Plus® reactor model. The kinetics has been validated with the model developed by comparing experimental and simulated data on the reduction reactor. The sensitivity of both the reduction and oxidation reactors have been performed. The reduction reactor temperature and pressure were varied between 1200-1600^oC and 10^{-3}-10^{-7} bar, respectively. The oxidation reactor was evaluated by varying the inlet temperatures of the reactants as well as the relative gas composition between CO_2 and H_2O. Results indicate a non-stoichiometry achievable from the reduction of ceria of 0.198 at 1600^oC and 10^{-7} bar vacuum pressure. In the oxidation reactor, water splitting yields significantly better solid conversion (metal oxide conversion) of 97%, as compared to 91% by CO_2 splitting with 5% excess gas flow than the stoichiometric requirements. The metal oxide inlet temperature significantly improves the yield of the oxidation reactor, in contrast to the minimal impact of variation of gas inlet temperature. A selectivity of over 90% can be achieved irrespective of gas composition with over 90% metal oxide conversion in the oxidation reactor.

Keywords: CO_2/H_2O dissociation, Chemical looping solar fuels, Moving bed reactor, reaction kinetics, simulation study.

1. Introduction

In recent years, synthetic fuels derived from carbon dioxide (CO_2) have been explored to lower the fossil carbon emissions. Re-use of CO_2 via catalytic processes for hydrocarbons and alcohol production, to be used in industrial applications has been proposed (Cuéllar-Franca and Azapagic, 2015; Zimmermann and Schom, 2017). Thermochemical conversion of CO_2 to fuels harnessing solar energy by concentrated solar power (CSP) systems is an interesting alternative (Aresta et al., 2013; Meylan et al., 2015). The CSP supplies the high temperature necessary for conversion reactions (usually, chemical looping redox cycles), hence producing syngas.

Thermochemical cycles have been studied since the early 1960s with the focus on developing materials for nuclear reactors. However, their use within the production of synthetic fuels as a low emission technology tremendously increased after the Kyoto protocol (Yadav and Banerjee, 2016). Numerous thermochemical cycles have been proposed comprising multiple steps. Of them the two-step redox oxide pair systems have shown great potential for synthetic solar fuel generation (Farooqui et al., 2018). These thermochemical cycles operate on the principle of transition between higher valence oxidized (MeO_{oxd}) and lower valence reduced (MeO_{red}) form of the oxide of a metal having multiple oxidation states (Agrafiotis et al., 2015). A generic chemical looping unit layout based on the solar thermal reduction of the metal oxide is shown in Figure 1. The first higher temperature endothermic step requires a higher valence metal oxide to undergo thermal reduction (TR). Therefore, oxygen is released because of the supply of external heat to form a lower valence metal oxide of the same. In the second step, the reduced metal oxide is oxidized back to higher valence state by accepting oxygen from water and/or CO_2. This in turn, results in H_2 and CO production by reactions called water splitting (WS) and carbon dioxide splitting (CDS), respectively (Roeb et al., 2012).

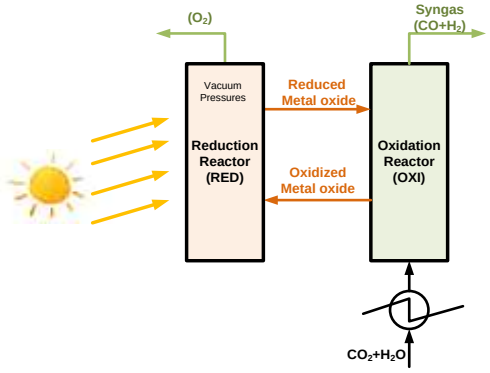

Figure 1. Schematics of interconnected solar-driven thermochemical CO_2 and H_2O dissociation.

Many metal oxide redox pairs, also called oxygen carriers (OC) have been exploited in the recent years to investigate the behaviour and the reactivity of materials for enhancing splitting reactions. Of them, ZnO, SnO_2, Fe_3O_4, and CeO_2 are the most common (Steinfeld, 2005). It is observed that ceria exhibits excellent optical and electrochemical properties with large oxygen carrying capacity. In addition, its ability to release and accept oxygen in response to temperature and oxygen chemical potential variations, makes it a suitable candidate as an oxygen carrier for thermochemical dissociation of CO_2/H_2O (Wheeler et al., 2018). Furthermore, its ability to undergo non-stoichiometric redox reactions ($CeO_2 \rightarrow CeO_{2-\delta}$) reduces the reduction temperature significantly. Though doped ceria and perovskites have also been recently explored due to their high oxygen storage capacity at a relatively lower temperature than undoped ceria (Scheffe and Steinfeld, 2014), requirement of costly dopants or the scarce availability of perovskites in large scale limit the usage compare to ceria that is readily available at lower cost.

The reaction conditions, including temperature, partial pressure of reactants during both the oxidation and reduction plays a crucial role in the overall reaction kinetics. This

in turn significantly influences the overall process performance and the corresponding efficiency. As to the best of the authors' knowledge, limited literature exists in predicting the performance of the thermochemical cycles considering non-structured reactor systems. Addressing this gap in the literature, this paper developed a comprehensive integrated kinetic-based moving bed reactor model and applied it to simulate both the syngas production from water and carbon dioxide by oxidation and the thermal reduction of the metal oxide. Following the selection of a suitable reactor configuration, the kinetics were implemented using FORTRAN subroutine and included in the reactor model developed in ASPEN Plus®. Sensitivity assessments were further performed to evaluate the relevance of different working parameters including the temperature, pressure, reactor volume, inlet gas composition of the respective reactors and validated for the reduction application by comparing simulations with experimental results.

2. Reaction Kinetics

The typical reactions taking place in the reduction and the oxidation reactors are shown below in equations (1) and (2). In these, at first, ceria releases oxygen and undergoes thermal reduction, in turn, to be oxidized by the incoming carbon dioxide and/or water producing carbon monoxide and hydrogen respectively. Also, the two reactions are fundamentally different from the energy perspective. While the former is endothermic, the latter is an exothermic reaction. Hence, the reduction reactor is most often operated at a much higher temperature than the oxidation reactor.

$$\text{Reduction reactor}: CeO_2 \xrightarrow[T_1]{\Delta H_1} CeO_{2-\delta} + 0.5\delta O_2 \quad (1)$$

$$\text{Oxidation reactor}: CeO_{2-\delta} + \delta CO_2 \xrightarrow[T_2]{-\Delta H_2} CeO_2 + \delta CO \quad (2a)$$

$$\text{Oxidation reactor}: CeO_{2-\delta} + \delta H_2O \xrightarrow[T_2]{-\Delta H_2} CeO_2 + \delta H_2 \quad (2b)$$

A maximum non-stoichiometry without changing the fluorite structure of CeO_2 for redox recycling of ceria was thus reported to be 0.286 ($1.714 \leq (2-\delta) \leq 2.0$) at 1000°C (Chueh and Haile, 2010). On the other hand, Bulfin et al. (Bulfin et al., 2013) developed an analytical thermal reduction model, where the maximum δ (δ_{max}), was obtained as 0.35 with least standard deviation below 1600°C. In this context, due to the limited availability of the thermodynamic properties of non-stoichiometric ceria, a different approach was used to describe the reactions. The fully reduced and stable form of ceria, Ce_2O_3, whose properties are widely available in the literature was thereby used. With this consideration, the above reaction set of thermal reduction of ceria and corresponding oxidation by CO_2 and H_2O (equations 1 and 2) could therefore be re-written respectively by Eq. (3-5) as follows.

$$CeO_2 \xrightarrow{k_{red}} (1\text{-}2\cdot\delta)CeO_2 + \delta Ce_2O_3 + 0.5\delta O_2 \quad (3)$$

$$(1\text{-}2\cdot\delta)CeO_2 + \delta Ce_2O_3 + \delta CO_2 \xrightarrow{k_{oxd}} CeO_2 + \delta CO \quad (4)$$

$$(1\text{-}2\cdot\delta)CeO_2 + \delta Ce_2O_3 + \delta H_2O \xrightarrow{k_{oxd}} CeO_2 + \delta H_2 \quad (5)$$

where the non-stoichiometry factor, δ, is the ratio between the completely reduced form of ceria, Ce_2O_3, and the still unreacted ceria, i.e., CeO_2.Based on equation (3), this can thus be evaluated by equation (6), whereby the value of δ varies between 0 and 0.5, the later corresponding to a fully reduced state of CeO_2

$$\delta = \frac{\dot{n}_{Ce_2O_3}}{2 \times \dot{n}_{Ce_2O_3} + \dot{n}_{CeO_2}} \quad (6)$$

Degree of advancement of reaction has been used in the kinetics model developed instead of the non-stoichiometry coefficient. This is to overcome the limited availability of the thermodynamic properties of non-stoichiometric ceria at different δ values Therefore, a separate parameter X was defined for all the reactions in terms of the relative content of Ce_2O_3 and CeO_2 in the solid mixture after respective reactions. For the reduction of CeO_2, the degree of advancement of reaction X_{RED} primarily describes the performance of the reduction reaction in terms of degree of reduction of the ceria powder as shown in equation (7). The equation is based on its relationship with the non-stoichiometry coefficient δ, whereby a maximum extent of reaction is obtained at δ_{max} of 0.35 assumed after the results reported by (Bulfin et al., 2013). The numerator represents the current non-stoichiometry after reduction, while the denominator indicates the maximum possible non-stoichiometry.

$$X = X_{RED} = \delta / \delta_{max} \quad (7)$$

A detailed discussion on the calculation of the degree of advancement of reaction is done in the following subsections. Indeed, such formulation of the degree of advancement of thermal reduction reaction (X_{RED}) agrees with the reduction kinetic model developed by Bulfin et al (Bulfin et al., 2013). On the other hand, the oxidation of the reduced ceria inherently moves in the opposite direction to reduction, whereby, the extent of oxidation (X_{OXI}) can be written according to the following equation (8).

$$X_{OXI} = 1 - X_{RED} \quad (8)$$

Before delving into detail at the individual reaction kinetics, the pathways of reaction are worth discussing. Two primary pathways of reaction for the solid-gas systems have primarily been used in the literature (Levenspiel, 1999a). In one reaction mechanism, the solid particle decreases in size as the reaction moves forward and leaves only a small portion containing impurities that are unable to react. An example being coal combustion, where the unreacted fraction of the initial fuel remains as ash. Another example of such a mechanism might be a reduction of volatile OCs, whereby the metal oxide gets vaporized after the removal of oxygen by thermal reduction. The second mechanism assumes a constant reaction particle size during the entire reaction, even though the composition changes. The non-volatile OCs can essentially be considered to follow this reaction approach when the temperatures are low enough not to cause sublimation of the outer layers of the solid (Abad et al., 2009; Chen et al., 2017).

The thermal reduction of metal oxides comprises several reaction steps. In the five step mechanism described by Levenspiel (Levenspiel, 1999b), the first two step, which are diffusion of reactant through the film surrounding the surface of the ceria particle and penetration and diffusion of reactant through the blanket of ash to the surface of the unreacted core, will be absent. Only the release of oxygen due to thermal reduction at the surface of the ceria, followed by the diffusion of oxygen through the ash layer (intraparticle diffusion) back to the exterior surface of the ceria are present. Then, the diffusion of oxygen through the gas film (external mass transfer) back to the external body of the fluid is the final step of the reaction mechanism.

Shrinking core model (SCM) can be used to model the redox kinetics of ceria, though is not often used due to its complexity. Most of the studies focused on the kinetics of the OCs tend to describe possible reaction pathways for the material and later try to fit experimental data into various reaction models, based on the rate-limiting step in the reaction. Thus, the rate-determining step of the reaction pathway is included in the general formulation of the reaction rate. Between the two reactions, the reduction reaction being inherently slower, is the rate-determining step for the entire cycle. This also directly influences the yield from the oxidation step. Efficient oxygen exchange between redox cycles can be achieved by creating mesoporous or microporous forms of structures of ceria with shorter bulk diffusion lengths, higher surface area and increased porosity (as it helps in radiative heat transfer) (Davenport et al., 2017; Ji et al., 2017). It is reported that the rate determining in thermochemical redox cycle would either be gas-phase limited or surface kinetics (Davenport et al., 2016; Ji et al., 2016). For temperature above 1100^{o}C the rate determining is gas-phase limited dynamics (also called thermo-kinetic controlled or quasi-equilibrium behavior) due to the bulk oxygen diffusion, while surface reaction is very fast with negligible impact on the overall rate. For oxidation step with high normalized gas flow rate, low temperature (below 1000^{o}C), or low specific surface area, the surface reaction is the rate-limiting step (Chueh and Haile, 2010). Therefore, based on the above discussions, as well as considering that the crystal structure of the OC, especially for non-volatile and non-stoichiometric ceria remains constant throughout the redox cycle, a simplified approach was considered for modelling the reaction kinetics for the solar thermochemical cycle as described in the following sub-section.

2.1 Reduction kinetics

Bulfin et al. (Bulfin et al., 2013) investigated ceria reduction kinetics for a wide range of temperatures, between 1000^{o}C and 1900^{o}C and a wide range of oxygen partial pressures from 10^{-2} to 10^{-8} bar. The partial pressure of oxygen derives from the presence of removable oxygen produced by the reduction of CeO_2 as per equation (3).

The proposed reduction kinetic model by Bulfin et al. (Bulfin et al., 2013) is essentially based on the Arrhenius equation, assuming an equilibrium reaction. This causes both forward and backward reactions, i.e. the release of oxygen and the recombination of released oxygen, to occur together ($CeO_2 \leftrightarrow CeO_{2-\delta} + 0.5\delta O_2$).

The oxygen vacancy concentration change during the reduction reaction is the rate at which oxygen departs from CeO_2 (forward reaction), less the rate at which it again

combines (backward reaction). This is given by the following equation (9), which can be further rewritten to non-dimensional form as equation (10).

$$\frac{d[O_{vac}]}{dt} = [O_{Ce}]k_f - [O_{vac}][O_{gas}]^{n_b} k_b \quad (9)$$

$$\frac{1}{[Ce]}\frac{d[O_{vac}]}{dt} = \frac{[O_{Ce}]}{[Ce]}k_f - \frac{[O_{vac}]}{[Ce]}[O_{gas}]^{n_b} k_b \quad (10)$$

where, [Ce], [O_{Ce}], [O_{vac}], [O_{gas}] are the cerium concentration, oxygen that can be released from ceria, vacancies of the oxygen and oxygen gas concentration that is released, respectively; k_f and k_b are forward and backward reaction rate constants. It is also mentioned that the rate constants were based on Arrhenius-type equation which relates temperature with activation energy and pre-exponential factors. Unlike the previous argument described in equation (6), (7) and (8) of measuring the extent of non-stoichiometry, it was proposed that moles of oxygen vacancies [O_{vac}] per mole of cerium [Ce] per second – or simply per second – to be used as the measure of the non-stoichiometry of the reduced ceria, as shown in the following equation (11).

$$\frac{[O_{vac}]}{[Ce]} = \delta \quad (11)$$

The forward reduction reaction is driven by the concentration of oxygen removal, while the backward recombination (or oxidation) reaction is influenced by the concentration of both the vacancies and the oxygen (Bulfin et al., 2013). Thus, the rate of the total change of the non-stoichiometry, which in other terms is also the rate of change of the oxygen vacancy concentration can be written in a similar manner to equation (9) as difference of the rate at which oxygen leaves CeO_2 (forward reaction) and the rate at which it recombines (backward reaction) as per the following equation (12). The overall process is depicted in the following Figure 2.

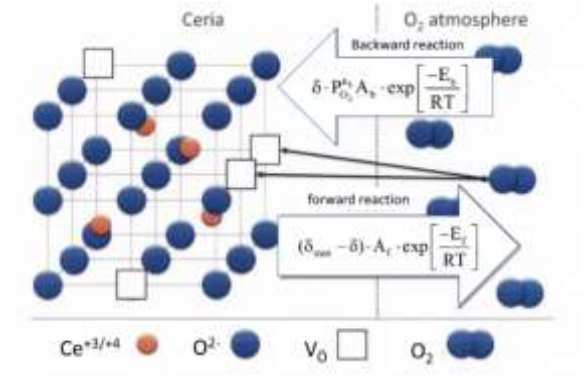

Figure 2. Reduction equilibrium reaction considering forward and backward reaction (Bulfin, 2015).

$$\frac{d\delta}{dt} = (\delta_{max}-\delta)\cdot A_f \cdot \exp\left(-\frac{E_f}{RT}\right) - \delta \cdot P_{O_2}^{n_b} \cdot A_b \cdot \exp\left(-\frac{E_b}{RT}\right) \quad (12)$$

where A represents the Arrhenius constant, E is the activation energy in kJ/mol/K, P_{O_2} is the partial pressure of oxygen, n_b is the reaction order, R is the universal gas constant and T is the absolute temperature in Kelvin with subscript f and b as forward and backward reaction respectively.

Assuming ideal gas behaviour, the concentration of O_2 is directly proportional to the partial pressure of O_2 (P_{O_2}) in the presence of sweep gas, or the vacuum pressure of the reactor, as applicable based on the reactor design. Based on the works of Panlener et al. (Panlener et al., 1993) and Dawicke et al. (Dawicke and Blumenthal, 1986) and through the plotting of log(δ) against log(P_{O_2}) with certain assumptions, the authors developed a reaction kinetic model for the net thermal reduction reaction of ceria. To fit the developed kinetic model with the experimental results, the shrinking core model was used. Considering a surface reaction to be the rate-determining step there would be a shrinking sphere of vacancies resulting in a restriction on the reaction rate with the advancement of the reaction. A third order model for the rate equation was found to be the best fit and the overall rate equation for the reduction reaction, based on X_{RED} is obtained as per the following equation (13).

$$\frac{dX_{RED}}{dt} = \frac{d\delta}{dt} \cdot (1\text{-}X_{RED})^{-1/3} \tag{13}$$

The values of the parameters of the rate equation are summarized in Table 1

Table 1. Ceria reduction rate equation coefficients presented by Bulfin et al. [27]

Parameter	Value
δ_{max}	0.35
n_b	0.218 ± 0.0013
E_f (kJ/mol)	232 ± 5
E_b (kJ/mol)	36 ± 4
A_f (s^{-1})	720,000 ± 360,000
A_b ($s^{-1}bar^{-n}$)	82 ± 41

The transition from the rate equation to the reaction rates of the concerned chemical species is done as per the equations (2) and (13) together with the available chemical species. Three distinct chemical species take part in the above reaction. For each mole of cerium (III) oxide (Ce_2O_3) generated, two moles of ceria (IV) oxide (CeO_2) are consumed and half a mole of oxygen gets released. Aside from stoichiometric coefficients, knowledge of reaction time step is important. In the discrete kinetic model, the particle residence time is used as the time parameter, in terms of Δt, as can be seen from equations (14) through (16). The thermal reduction reaction rates for the three species taking part in the reaction are shown below.

$$k_{RED\text{-}CeO_2} = -2 \cdot \dot{n}_{CeO_2} \frac{dX_{RED}}{dt} \Delta t \tag{14}$$

$$k_{RED\text{-}Ce_2O_3} = 1 \cdot \dot{n}_{\dot{n}_{CeO_2}} \frac{dX_{RED}}{dt} \Delta t \quad (15)$$

$$k_{RED\text{-}O_2} = 0.5 \cdot \dot{n}_{\dot{n}_{CeO_2}} \frac{dX_{RED}}{dt} \Delta t \quad (16)$$

where $k_{RED\text{-}i}$ is rates of reduction species i listed as CeO_2,Ce_2O_3,O_2.

2.2 Oxidation kinetics

The oxidation kinetics for ceria for H_2O and CO_2 splitting have been investigated by several research groups (Ackermann et al., 2015; Arifin and Weimer, 2018; Farooqui et al., 2018). The initial reduction state of the sample has been reported to strongly influence the subsequent oxidation reaction. A significant drop in the reaction rates was noticed when non–stoichiometry factor exceeded 0.18-0.2 values in the temperatures below 820ºC (Ackermann et al., 2015). High variations in the reaction activation energies are reported with non–stoichiometry of the sample in higher concentrations of the oxidizing gas. As reported, the activation energy varied in the range of 160-200 kJ/mol for non–stoichiometry between 0.01 and 0.09. For oxidation kinetics, Arifin (Arifin, 2013) and Arifin and Weimer (Arifin and Weimer, 2018) investigated a redox kinetics of ceria for water and carbon dioxide splitting reaction. The reaction mechanism has been proposed in the general formulation for the reaction rate as equation (17) with the corresponding coefficients being listed in Table 2.

$$\frac{dX_{OXI}}{dt} = A_0 \cdot \exp\left(-\frac{E_0}{RT}\right) \cdot y_i^{n_o} \cdot (1 - X_{OXI})^{\psi} \quad (17)$$

where A_0 is the Arrhenius constant, E_0 is the activation energy degree and n_o is the order of the oxidation reaction and y_i is the oxidant molar fraction. The oxidation reaction of the reduced ceria with water vapour and CO_2 splitting was found to behave similarly to a homogeneous reaction, i.e. its rate decelerates proportionally to the depletion of the reactants ($1\text{-}X_{OXI}$). However, unlike the water-splitting reaction, that presents a relatively faster reaction with a low activation energy of 29 kJ/mol, the CO_2 splitting reaction is a more complex phenomenon based on surface mediation.

Similar analyses revealed the dependence of the rate-determining step of the carbon dioxide splitting reaction on the temperature of the process (Arifin, 2013). It was also observed that with the increase in temperature, carbon site blocking, and subsequent surface recombination stops. At 875ºC the only reaction pathway is the direct desorption of carbon monoxide from the particle surface, which might result in significant changes to the reaction coefficients ψ and n_o as indicated in Table 2. It is worth noticing that in the discussed research, ceria sample was constantly cycled and reused in different conditions. Nevertheless, Arifin (Arifin, 2013) noted that the overall production of the fuel from the sample remained almost constant, though reaction times varied because of varying temperatures and molar fractions of reactants.

Table 2. Kinetic parameters of the oxidation reaction of reduced ceria obtained by Arifin and Weimer (Arifin and Weimer, 2018)

Oxidant	Temp (ºC)	A_0 (1/s)	E_0 (KJ/mol)	ψ (-)	n_o(-)

CO_2	750-950	1.0	29	0.89	1.0
	650-725	4.2	47	0.53	1.0
H_2O	750-800	3.4	45	0.65	1.2
	825-875	2.5	41	0.7	1.7

To determine the reaction rates for splitting reactions, the degree of advancement of oxidation reaction was calculated as per mentioned in equation (8). Following the aforementioned equation, independent to the use of CO_2 or H_2O, when one mole of each species is consumed, it leads to simultaneous consumption of one mole of Ce_2O_3 with corresponding generation of two moles of ceria and one mole of CO and H_2 respectively. Taking this into account, the reaction rates for each species, in terms of the available solid reactant quantity (molar flow) are listed as per the following equations (18-23).

$$k_{OXI\text{-}CeO_2} = 2 \cdot \dot{n}_{Ce_2O_3} \left\{ \frac{dX_{OXI\text{-}H_2O}}{dt} + \frac{dX_{OXI\text{-}CO_2}}{dt} \right\} \Delta t \quad (18)$$

$$k_{OXI\text{-}Ce_2O_3} = -1 \cdot \dot{n}_{Ce_2O_3} \left\{ \frac{dX_{OXI\text{-}H_2O}}{dt} + \frac{dX_{OXI\text{-}CO_2}}{dt} \right\} \Delta t \quad (19)$$

$$k_{OXI\text{-}H_2O} = -1 \cdot \dot{n}_{Ce_2O_3} \frac{dX_{OXI\text{-}H_2O}}{dt} \Delta t \quad (20)$$

$$k_{OXI\text{-}H_2} = 1 \cdot \dot{n}_{Ce_2O_3} \frac{dX_{OXI\text{-}H_2O}}{dt} \Delta t \quad (21)$$

$$k_{OXI\text{-}CO_2} = -1 \cdot \dot{n}_{Ce_2O_3} \frac{dX_{OXI\text{-}CO_2}}{dt} \Delta t \quad (22)$$

$$k_{OXI\text{-}CO} = 1 \cdot \dot{n}_{Ce_2O_3} \frac{dX_{OXI\text{-}CO_2}}{dt} \Delta t \quad (23)$$

where $k_{OXI\text{-}j}$ is the rate of oxidation species j listed as CeO_2,Ce_2O_3,H_2O, H_2, CO_2, CO.

3. Model development

Based on work of Panlener et al. (Panlener et al., 1993) and following the kinetics developed by Bulfin et al. (Bulfin et al., 2013), which has also been used in the present study, it can be concluded that a very low partial pressure of oxygen is necessary to have an acceptable reduction of ceria. Often, this can be a pressure lower than 10^{-5} bar (Bulfin et al., 2013), corresponding to the temperatures of 1300^{o}C and above. Such a low pressure can be achieved either by operating the reactor in vacuum conditions or by sending sufficiently high sweep gas flow to maintain the desired level of oxygen partial pressure in the reduction reactor. The later, however, requiring more than 10^5 times the sweep gas flow with respect to the oxygen delivered, is often limited due to the scale of the amount of inert gas flow. The moving bed aerosol reactor, proposed by Scheffe et al. (Scheffe et al., 2014), acknowledges this fact, which would lower the effectiveness of the entire cycle. Indeed, such requirement of low pressure for direct reduction limits the use of

sweep gas, which in turn would limit the application of fluidized bed reduction reactors. On the other hand, non-structured reactors working under vacuum can essentially be referred to as equivalent to moving bed reactors, where the particles undergo reduction while moving through the reactor. Reactor design concepts by Muhich et al. and Ermanoski among many other similar reactor designs proposed are essentially of this type (Ermanoski et al., 2013a, 2013b; Ivan Ermanoski, 2013; Muhich et al., 2016).

On the other hand, it is essential to maintain higher pressure to perform the oxidation. With CO and H_2 being the primary products, this would considerably decrease the work needed for the compression of the products, especially H_2, essential for their downstream industrial applications. In this regard, both fluidized bed and moving bed reactor configurations are applicable with relative advantages and disadvantages. While the circulating fluidized bed provides a major solution to the challenge of transporting metal oxide between the reactors, purity of the products and fluidization regime is a significant disadvantage. Fan et al. (Fan, 2017) studied and reported the relative advantages of a moving bed reactor over a fluidized bed reactor for reduction of oxygen carriers with methane. Besides a more homogeneous reduction of the OCs, reactions in a moving bed reactor result closer to thermodynamic equilibrium.

In a fluidized bed reactor, due to the requirement of desired flows for fluidization, this often results in a low gas or metal oxide conversion (transport reactors for smaller configurations) or would require sufficiently large reactors with a very high oxygen carrier inventory (bubbling bed reactors). Additionally, for transport reactors, the relative gas conversion is very low with a low-pressure drop, while for a bubbling bed, even though the conversion is higher, would result in a higher pressure drop. A low gas purity would then require downstream purification before the use of the generated product for the subsequent industrial application. However, the effectiveness of the cycle decreases. Moving bed reactors, on the other hand, do not experience such limitations and hence provides better flexibility in design and operation (Ermanoski et al., 2013b; Ivan Ermanoski, 2013)

Following the above discussions, moving bed reactor model was developed for both the reduction and oxidation reactions. . The reduction reactor would favourably operate under vacuum, whereas the oxidation reactor would perform optimally at near atmospheric conditions. This resembles the reactor concept proposed by Muhich et al. (Muhich et al., 2016), with the only essential difference being that the oxidation reactor is a moving bed reactor instead of a bubbling bed reactor. The transport of the oxidized metal oxide particle can be performed by a screw-conveyor.

The present study has been focused on the development of the reactor model using commercial software ASPEN Plus® to predict the results reported in literature and to investigate the performance of each reactor for different operating conditions in order to have a high purity of the syngas produced and to see the effect of composition of mixture (CO_2 and H_2O) on the conversion within the oxidation reactor. The following section details the development of such reactor models and the obtained results are discussed in Section 4.

3.1 Moving bed reactor model

A general schematic of the countercurrent moving bed reactor is shown in Figure 3. In the vacuum operated reduction reactor, the metal oxide is thermally reduced, as it travels through the reactor from the top. Hence, no separate gas inlet is necessary. The generated oxygen flows up to the top of the reactor in a counterflow with respect to the metal oxide, wherefrom it is connected to a vacuum pump that drives it away and maintains the necessary vacuum (not shown). In the oxidation reactor, the reduced metal oxide is fed from the top as well and reacts with the gas (CO_2/H_2O) moving up. Since the splitting reaction is exothermic, a temperature gradient exists along the length of the reactor for non-isothermal operations. The reduced metal oxide is removed from the bottom (e.g., by a rotating grate, not shown in the figure), while the produced gas exists the reactor from the top. The oxidized metal oxide is transported back to the reduction reactor. The pressure swing between the two reactors for the metal oxide has been proposed to be performed similarly to the one proposed by Muhich et al (Muhich et al., 2016) in their reactor design concepts. At the bottom of the reduction reactor, the particles would be stored, in a form replicating a pseudo packed bed, before being transmitted into the oxidation reactor via a constricted passage. This pseudo-packed bed moving storage, together with a gradually decreasing flow area would provide the necessary pressure buffer, so as to increase the pressure from the vacuum in the reduction reactor to nearly atmospheric pressures in the oxidation reactor. However, since it is a physical process, it would not lead to additional mechanical work being expended.

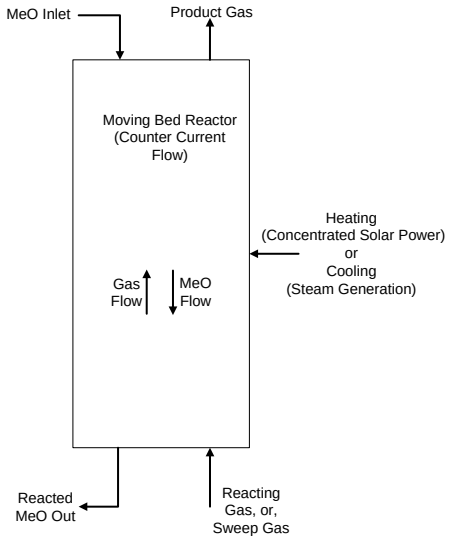

Figure 3. Schematic diagram of a generic moving bed reactor

A common approach to the modelling of moving bed reactors is to use commercial process flowsheet simulators, implementing thermodynamics or kinetics reaction models. This can be coupled to several types of in-built reactor models, which can be further integrated in system models for the simulation of complete processes. In the literature, the most common commercial software applied for reactor modelling is ASPEN Plus®. Since no moving bed reactor model exists in ASPEN Plus®, the development of a comprehensive model using the available in-built reactor models of ASPEN Plus® is necessary. Benjamin (Benjamin, 1985) proposed a built-in model for a counter-current

moving bed coal gasifier, an analysis of which, can be found in the ASPEN guide to moving bed gasifier modelling (*ASPEN Plus Model for Moving Bed Coal Gasifier-Aspen Technology tutorial*, 2010). However, the complex model resulted in time consuming simulations. An alternative, as proposed by ASPEN Plus® user guide (*ASPEN Plus Model for Moving Bed Coal Gasifier-Aspen Technology tutorial*, 2010), is to utilize multiple RCSTRs (continuous stirred bed reactors) in series, resulting in a considerably simpler model. This also allows the direct use of the built-in algorithms of ASPEN Plus®. Such a reactor model for the thermodynamic assessment of a moving bed configuration was assessed by Tong et al. (Tong et al., 2013) for a chemical looping combustion cycle based on a moving bed reactor with Fe_3O_4/Fe redox pair and methane as fuel. Five RGIBBS reactors were modelled in series to simulate the counter-flow moving bed reactor, employing minimization of the Gibbs free energy for thermodynamic analysis. A good match for both the solid and gas conversion was obtained with respect to the experimental results reported in the same literature (Tong et al., 2013). Chang et al. (He et al., 2013) developed a steady state kinetic model of a moving bed gasifier using a similar approach in ASPEN Plus® to simulate a Lurgi Coal Gasifier for Synthetic Natural Gas (SNG) production. In the same study, the methodology for optimizing the number of RCSTRs in series – necessary to provide a convergence to the obtained results – was demonstrated. The results were also compared with industrial data, with good agreement.

A counter-current reactor model was thereby simulated for the thermal reduction and CDS and WS reactions respectively, using RCSTR reactors in series available in ASPEN Plus® database. The RCSTR reactor has the characteristic that all phases have the same temperature, which means the temperatures of solid and gas phases in the reduction and oxidation processes are equal in each RCSTR model. Also, it is modelled so that each RCSTR has the same volume, equal to the whole gasifier volume divided by the number of RCSTRs in series. The reaction kinetics described were written in an external user kinetic subroutine in FORTRAN, which is compiled and hooked up with each of the RCSTR reactors in the moving bed model. Specific assumptions with respect to the oxidation and reduction reactors were individually considered and summarized below:

1. All the RCSTRs in the reduction reactor were at the same temperature, to simulate an isothermal reactor for the reduction.
2. No heat losses were considered in the RCTSRs comprising the oxidation reactor i.e., they were assumed to be adiabatic reactors. This drives the temperature of the products and the reactor in some cases quite high. If not controlled, this might lead to the change of crystal structure of the oxygen carrier in actual practice. However, such considerations were not considered during the present simulation.
3. A single-entry, counter-current moving bed reactor was simulated for the oxidation reactor, where the oxygen carrier is fed from the top and the reactant gas flows upward from the bottom inlet as shown in Figure 3. However, the scope for optimization to enhance the reaction rates, together with performing temperature control within the reactor by multiple gas inlets is possible. Nevertheless, it was not included in the present study.

4. The residence time in the reactors was calculated based on the bed volume with respect to the inlet oxygen carrier volumetric flow rate neglecting the changing volume flow due to change in composition from reactions.
5. No change in oxygen carrier structure and hence the change in reactions kinetics was considered during the course of the reactions.

Modelling a moving bed reactor with a series of RCSTRs is like discretizing the reactor volume in a finite number of smaller volumes. Indeed, the higher the number of RCSTRs in series, the higher is the accuracy of the estimation of the yields from the reactor. But an excessive number of reactors would increase the iterative calculations resulting in a time-consuming simulation (Badillo-Hernandez et al., 2013). Also, such configurations exhibit slow solution convergence because of the form of the mathematical model of counter-current moving bed reactor, leading to a two-point boundary value problem (He et al., 2013). Hence, the selection of the number of RCSTRs in series is crucial to the net evaluation of the system in order to realize the goal of minimizing simulation errors and at the same time limiting the computation time as much as possible. To evaluate the number of RCSTRs in series that would result in the minimization of error from approximation, an iterative calculation procedure is applied, as described in Section 3.3.

The hook-up logic between the in-built ASPEN Plus® model and the external FORTRAN code for user kinetics, together with the use of calculator blocks for calculating the necessary external heat requirement for the isothermal reduction reactor is shown in Figure 4. Each RCSTR block is linked up with the user kinetic model and the resulting output is fed to the successive reactor. There will be exchange of variables from each RCSTR providing temperature, pressure and molar flow of each gaseous and solid species, along with the volume of each RCSTR, which are used in the FORTRAN subroutine to calculate non-stoichiometric parameter and metal oxide conversion. User-kinetic subroutine calculates the instantons rate of reaction (equation 13 and 17 for reduction and oxidation respectively) together with residence time. From instantaneous rate of reaction, rate of reaction of specific species is evaluated by equations (14-16) for reduction reaction and equation (18-23) for oxidation reaction, which are reported back to RCSTRs in Aspen Plus, as it can be seen in Figure 4b.

Unlike the reduction reactor, it is interesting to note that for the oxidation reactor, since two inlets (i.e., ceria and H_2O/CO_2 streams) at two different points in the reactor system are provided, the convergence is essentially a two-point convergence. This requires providing an estimation of the yields in each stream to facilitate convergence, and estimations too far off from the results often lead to increased convergence time and in some cases, failure of convergence.

Calculator blocks were added to calculate the heat need of each reactor for both the reduction and oxidation reactors. Then, besides the heat requirement, the need to calculate the non-stoichiometry (δ) generated along the length of the reactor, together with other parameters, might necessitate the addition of more calculator blocks for both the set of reactors. Indeed, based on the following Figure 4, the need to optimize the number of RCSTRs in series so as to predict well the net output from the RCSTR is essential and is conducted accordingly. The Broyden Solver was used as per the suggestion of ASPEN Plus® model already developed for moving bed coal gasifier (*Aspen Plus Model for*

Moving Bed Coal Gasifier-Aspen Technology tutorial, 2010) and 500 iterations were provided for both the mass and energy solvers. The relative tolerance of errors was set at 10^{-3} to decrease the computation time while minimizing errors in the overall results of the simulation. Usually, for gas processing, it is recommended to use the PR-BM method which utilizes the Peng-Robinson cubic equation of state with the Bostone Mathias alpha function (Fan et al., 2016). Therefore, the PR-BM method was selected for the simulations.

The temperature profile for an adiabatic reactor (oxidation) can be obtained through the results of each reactor, retrieved by calculator blocks. The corresponding non-stoichiometry of the input and the output metal oxide to the reactors are also evaluated via calculator blocks, incorporated with each RCSTR as per the coupling of the equations (6).

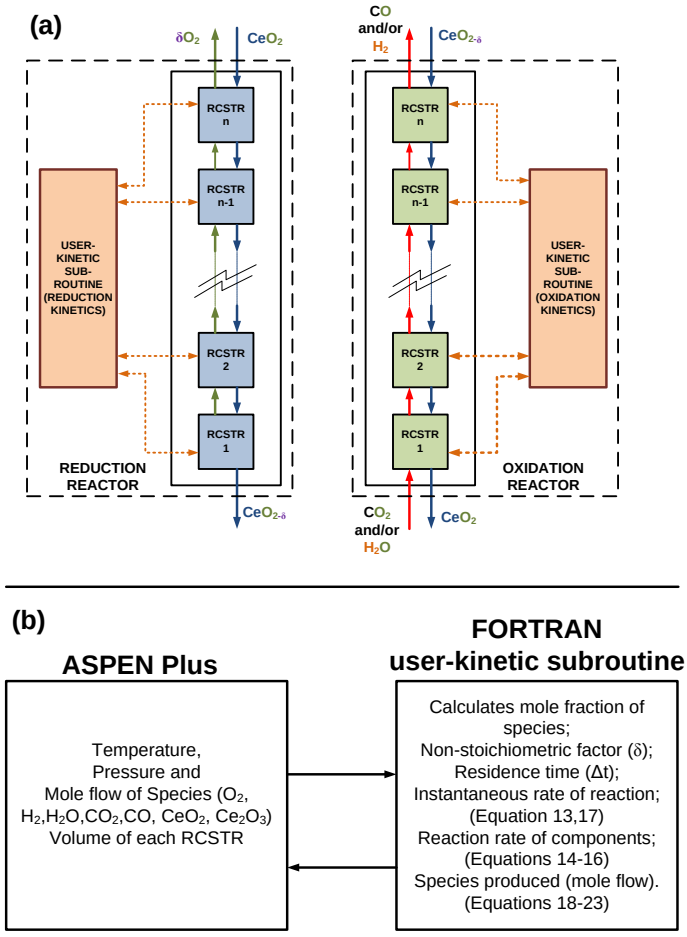

Figure 4. (a) Moving bed reactor model in ASPEN Plus® hooked with user-kinetic subroutine written in an external FORTRAN Code (b) exchange of variables between ASPEN Plus® and kinetic subroutine

3.2 Evaluation Methodology

Industrial-scale evaluation is essential to understand the design perspectives and evaluate the fundamental areas necessary for future focus for practical application of any chosen technology. In this regard, application of the chemical looping technology for CO/H_2 production, coupled to an industrial scale source of the CO_2 or water has been

evaluated. The reactor model has been evaluated based on the common aim to provide 100 mol/s of syngas from either CO_2 or H_2O or CO_2/H_2O mixture. The value suits well with the amount of CO_2 or water available from the state of the art carbon capture power plants (CO_2 Capture Project (CCP), 2015; Viebahn et al., 2015). As per equations (3 and 6), the equivalent amount of CeO_2 (with average diameter of 100 μm) to be circulated for generating a non-stoichiometry of 0.35 is 285.71 mol/s. This results in an equivalent Ce_2O_3 stream of 100 mol/s generated during the reduction phase, following the above-mentioned equations.

Solar Tower and Parabolic Dishes are the technologies of choice to achieve the high temperatures required (Agrafiotis et al., 2015). In addition, from the limitations of the scale with regards to parabolic dishes, the solar tower has been considered as the most suitable technology for thermochemical cycles. Nevertheless, till date, the highest temperature application for ceria cycles at 1600^{o}C through solar tower technology has been reported by Tou et al. (Tou et al., 2017). The reduction temperature was therefore varied between 1000^{o}C and 1600^{o}C to allow comparison of the results of the model developed with experimental results available in the literature. The base case for this reactor was selected also to be the best case application, with a temperature of 1600^{o}C and a reactor vacuum pressure of 10^{-7} bar, to obtain an acceptable reduction extent. Such low reduction pressures can be effectively achieved by cascading pressure chambers as suggested by (Brendelberger et al., 2017; Ehrhart et al., 2016; Ermanoski, 2014). The chosen operating pressure of reduction reactor is optimistic with respect to the vacuum technology available (and may require turbo vacuum pump) as the maximum generated vacuum would be limited by economic benefits achieved after integration with the power plants.

The oxidation reactor was evaluated separately from the reduction reactor to assist the present model development and evaluation. As has already been discussed, based on a maximum achievable δ of 0.35 (Wheeler et al., 2018), the oxidation reactor was supplied with a maximum reduced ceria. This was to ensure the study of the oxidation reactor, irrespective of the limitation to the reduction technologies. Furthermore, the kinetics of the oxidation reactor used in the present study had been evaluated at atmospheric conditions. However, by Le-Chatelier's principle, the oxidation reaction is preferred at higher pressures. Nonetheless, due to the uncertainty of the kinetics of reaction with pressure variation, a small pressure rise has been considered for the oxidation with respect to that at which the kinetics were developed. Hence, an oxidation pressure of 2 bar was selected for simulation study. This would also be advantageous through the decrease in the subsequent compression work associated with H_2 and CO compression for downstream applications. The gas flow rate was varied according to the need of the reactor design. This also results in the assessment of the product purity in the generated stream from the splitting oxidation reactor, better known as the selectivity. The selectivity of CO and H_2 via three different splitting reactions (only CO_2, only H_2O, and CO_2/H_2O mixture) is written as per the following equations 24(a) and 24(b).

$$S_{CO} = \frac{\dot{n}_{CO}}{\dot{n}_{CO_2} + \dot{n}_{CO}} \tag{24a}$$

$$S_{H_2} = \frac{\dot{n}_{H_2}}{\dot{n}_{H_2O} + \dot{n}_{H_2}} \quad (24b)$$

where ṅ represents the molar flow of the components in the outlet product gas from the splitting reactor (oxidation reactor) and the subscript represents the components for which the molar flows are considered.

In addition, the inlet temperature of the oxygen carrier into the reduction reactor was fixed at 1300^{o}C for the base case scenario. As for the oxidation reactor, the oxygen carrier and gas inlet temperature was fixed at 800^{o}C for base case simulations. Further sensitivity studies to evaluate the impact of the variation of these temperatures have been carried out and commented accordingly. Based on such assumptions and considerations, the following section details the results and the design aspects of the moving bed reactor for application to an industrial scale solar CO_2/H_2O splitting using ceria as the OC.

3.3 Model Convergence

To evaluate the number of RCSTRs in series that would result in the minimization of error from approximation, while also decreasing the simulation time, an iterative calculation procedure was adopted after He et al. (He et al., 2013). The reduction and the oxidation reactors have been considered separately for the optimization. Each RCSTR have been sequentially arranged along the height of the reactor, with an equivalent volume of 0.5 m^3 and 4 m^3 for the reduction and the oxidation reactor, respectively. An iterative procedure, with increasing the number of the RCSTRs (with the total volume of reactor fixed) is carried out until the relative change would result in a value lower than 0.25% change of the output (O_2 or H_2/CO flows) of the moving bed reactor. The value of 0.25% was considered a good approximation to the reactor convergence, while ensuring minimization of computation time by unnecessarily increasing the number of reactors in series. The schematic of the algorithm followed for the iterative simulation is shown in Figure 5.

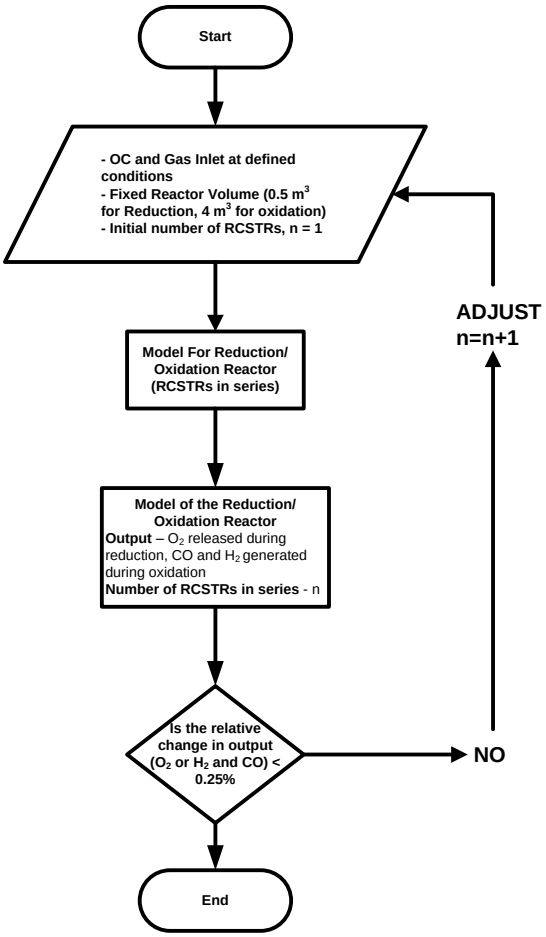

Figure 5. Iterative calculation procedure for determining RCSTRs numbers, n.

Figure 6 shows the relative changes of the outputs from the reduction and the oxidation reactors respectively while varying the number of RCSTRs in series (n). To evaluate the relative change, the oxygen released from the reduction of ceria was obtained for an isothermal reduction reactor at 1600^{o}C and a vacuum pressure of 10^{-7} bar. The amount of CeO_2 sent for reduction was 285.71 mol/s. As can be seen, beyond n = 4, the relative change in the results drops below 0.25% and beyond n = 7, the relative change becomes negligible. Therefore, the optimum number of RCTRs in the reduction zone is considered as n = 7.

For the oxidation reactor, the H_2 and CO yield was considered to evaluate the convergence of the number of RCSTRs. An equimolar mixture of CO_2/H_2O was sent to oxidize the reduced ceria with a maximum non-stoichiometric factor limit of 0.35, at a constant gas and metal oxide inlet temperature of 800^{o}C. As can be seen from the results shown in Figure 6b, due to slower CO_2 splitting kinetics, a larger number of RCSTRs in series is required to obtain the necessary convergence. Hence, while after 8 RCSTRs in series the relative change in H_2 yield drops below 0.25%, the corresponding value is obtained with 10 RCSTRs in series for the CO yield. Hence, an n = 10 was found to result in minimal relative error while simulating the Oxidation reactor.

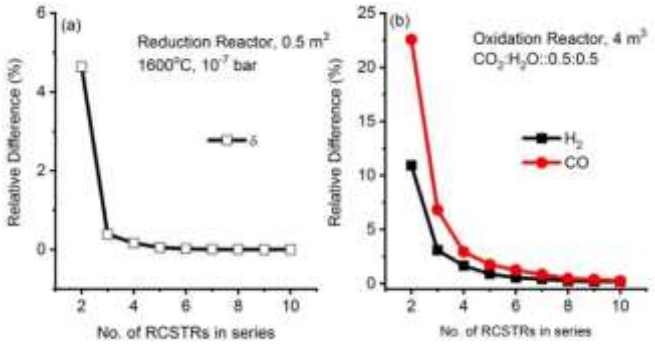

Figure 6. Relative changes in the output from increasing the number of RCSTRs in series for (a) Reduction Reactor (b) Oxidation Reactor

4. Results and discussion

4.1 Reduction reactor

The impact of the different operating parameters on the performance of the moving bed reduction reactor is described in the following section.

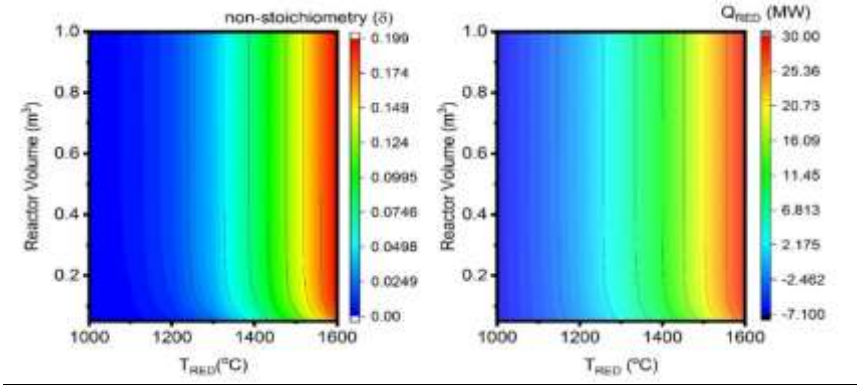

Figure 7. Variation of (a) Non-Stoichiometry (δ) and (b) heat requirement of the reduction reactor (Q) with temperature and reactor volume of the reactor at constant vacuum pressure of 10^{-7} bar, CeO_2 molar flow of 285.71 mol/s and metal oxide inlet temperature of 1300°C

The first sensitivity assessment was performed to evaluate the variation of the non-stoichiometry (δ) with respect to both the reactor volume and temperature of the reactor, as shown in Figure 7. Due to the increased rate of oxygen recombination reaction with an increase in the non-stoichiometry factor, a fast initial reaction is seen, especially at higher temperatures. However, the increase rate is slower for lower temperatures, where, the kinetics of the global reduction reaction is considerably slow. Therefore, no change in the reduction extent of ceria from a non-stoichiometry factor of 0.1982 is noticed at 1600°C beyond a reactor volume of 0.4 m^3, also signifying an approximate residence time of the metal oxide of 1.2 minutes within the reactor. On the other hand, for a lower temperature regime (< 1200°C), insignificant improvement is noticed with increase in the reactor volume even up to 1 m^3, corresponding to a residence time in the reactor of 3 minutes (see Figure S1 in supplementary file).

On the other hand, a higher reduction extent would result in a higher heat of reaction (Q_{RED}) in the reduction reactor. This is clearly depicted in Figure 7b, whereby a maximum Q_{RED} of 30 MW is needed to ensure the maximum yield of ceria reduction. Interesting to note is the negative heat required for operating at temperatures lower than 1200°C. Indeed, since the metal oxide inlet is fixed at 1300°C and no significant reaction is observed, a net cooling effect can be seen within the reactor, with the metal oxide releasing heat to reach 1200°C. However, above that temperature, a higher reaction extent occurs with high endothermicity, and this results in the net heat requirement for the reaction to increase and become positive. Nonetheless, an unnecessarily high reactor volume would require excess heating to the reactor, with minimal increase in the reduced ceria yield. Thus, choosing an optimal reactor volume would not only ensure an almost maximization in the desired yield over a wide range of temperatures but at the same time optimize the heat requirement of the reactor.

Hence, based on the above discussions, a reactor volume of 0.5 m^3 was selected to perform the subsequent sensitivity studies. Accordingly, the temperature of the reduction reactor was varied between 1000ºC and 1600ºC, while the vacuum pressure was varied between 10^{-3} and 10^{-7} bar to study the impact of temperature and pressure on the reduction of pure ceria. Figure 8 shows the obtained results, which are plotted together with the experimental data obtained from Bulfin et al. (Bulfin et al., 2013). As can be seen, a good agreement is obtained between the experimental results and the developed moving bed model in ASPEN Plus. Hence, a validation of the present model in predicting the non-stoichiometric reduction of ceria is obtained.

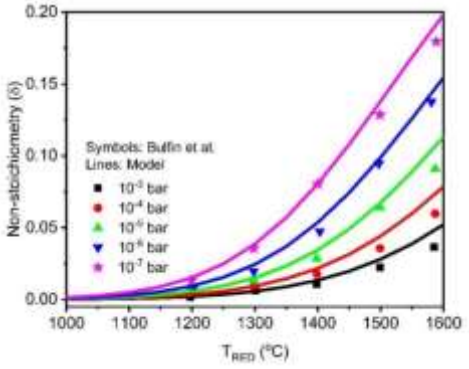

Figure 8. Variation of non-stoichiometry (δ) generated in the reduction reactor with temperature and reactor vacuum pressure at a constant reactor volume of 0.5 m^3, CeO_2 molar flow of 285.71 mol/s and constant metal oxide inlet temperature of 1300ºC. Symbols represent results of Bulfin et al. (Bulfin et al., 2013), lines represent the simulation model results.

Figure 8 further reveals that the profile of the non-stoichiometry (δ) with temperature is similar irrespective of the pressure variation. Below 1200ºC no significant reduction of ceria is noticed, even at a vacuum pressure of 10^{-7} bar. A steep increase in the non-stoichiometry (δ) of the reduction reaction is only noticed beyond 1300ºC. However, the rate of increase is enhanced at lower pressures, whereby the non-stoichiometry obtained at 1400ºC and 1500ºC being around 0.08 and 0.138 respectively for a pressure of 10^{-7} bar. Indeed, at the same two temperatures, the non-stoichiometry drops to 0.05 and 0.09 respectively at a lower vacuum pressure of 10^{-6} bar. The maximum non-stoichiometry of 0.199 was obtained at 1600ºC and a pressure of 10^{-7} bar. On the other hand, at lower

vacuum pressure, the reduction reaction becomes extremely limited, even at very high temperature , whereby only around 0.025 of δ was obtained at around 1475°C. The corresponding δ becomes around 0.06 and 0.124 at pressures of 10^{-5} and 10^{-7} bar respectively. Alternately, this also implies that to operate the reduction reactor at a lower vacuum condition, a higher temperature range needs to be maintained to have acceptable reduction yields. Therefore, the claim of the necessity to operate the reduction at high vacuum conditions, or, in other words, at very low partial pressures of oxygen is reinstated. This, however, provides an energy penalty from vacuum creation even though the corresponding yield increases.

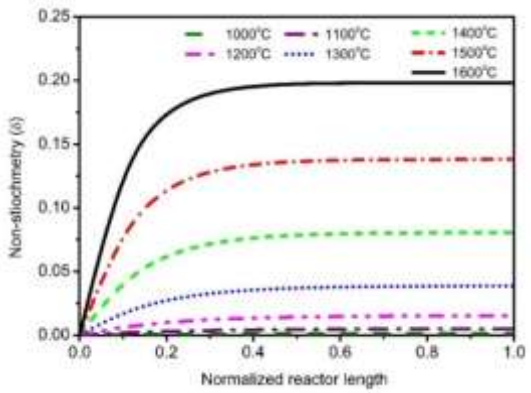

Figure 9. Variation of Non-Stoichiometry (δ) along the length of the reactor at a constant reduction reactor volume of 0.5 m^3, a constant CeO_2 flow of 285.71 mol/s and a constant reactor temperature and a vacuum pressure of 1600°C and 10^{-7} bar respectively.

The variation of the non-stoichiometry along the normalized length of the reactor is shown in Figure 9. For lower temperatures, below 1200°C, the evolution of δ along the length of the isothermal reactor is mostly linear. However, for temperatures of 1300°C and higher, most of the reaction occurs before half the reactor length. This can directly be followed from the discussed reactor kinetics, whereby the rates of the backward and the forward reaction becomes almost equal after an initial reduction of the ceria. Therefore, this implies that the reactor can either be made smaller in size, or the focus volume of the solar concentrator can be more concentrated to ensure the desired reaction while minimizing the solar energy input to perform the same.

In the end, the variation of the heat of reaction at a constant reduction temperature of 1600°C and pressure of 10^{-7} bar (plotted as the negative logarithm of the vacuum pressure) with a variable oxygen carrier inlet temperature is shown in Figure 10. Since the reactor has been modelled as an isothermal reactor, no change in the non-stoichiometry of the reduced metal oxide would occur with respect to the variable oxygen carrier inlet temperature to the reactor. As can be followed from previous arguments, at higher oxygen carrier inlet temperatures with a corresponding lower operating temperature of the reduction reactor, the net heat requirement for the reaction to occur decreases. Indeed, for a metal oxide inlet temperature of 900°C, the heat requirement increases by almost 20 MW to around 39.3 MW in relation to the base case oxygen carrier inlet temperature of 1300°C. Therefore, the importance of the metal oxide inlet temperature to the reduction reactor, which in other terms is the metal oxide outlet temperature from the oxidation

reactor, on the overall system performance is crucial, with a higher metal oxide inlet temperature resulting in a lower heat requirement in the reduction reactor.

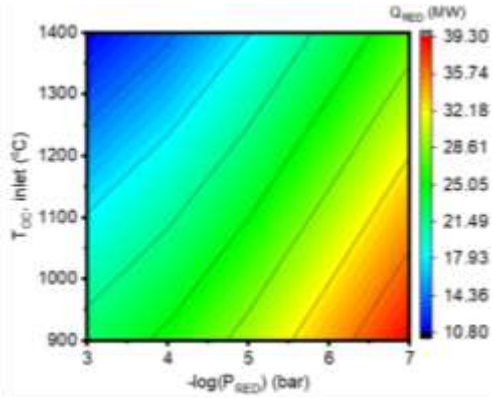

Figure 10. Variation of the heat of reaction (Q_{RED}) with metal oxide inlet temperature to the reduction reactor ($T_{oc, inlet}$) and reactor pressure for a constant reduction temperature of 1600°C for a constant reactor volume of 0.5 m^3 and CeO_2 molar flow 285.71 mol/s

4.2 Oxidation Reactor

After the sensitivity assessment on the reduction reactor, a complete set of sensitivity studies were performed on the moving bed oxidation reactor, as modelled in ASPEN Plus®. As discussed in the previous methodology section 3.2, a constant non-stoichiometry factor of 0.35 was assumed for the inlet to the reactor. For a CeO_2 flow of 285.71 mol/s, as assumed previously for the reduction reactor, this leads to the production of an equivalent of 100 mol/s of Ce_2O_3, as per discussed in equation (6). Besides, a constant metal oxide and gas feed temperature to the oxidation reactor (OXI) of 800°C was also assumed. A 5% excess of CO_2 or H_2O or CO_2/H_2O mixture was sent for CO or H_2 production respectively. The composition of the mixture was varied between five mixture compositions, more specifically 100% CO_2, 75% CO_2 and 25% H_2O, 50% each of CO_2 and H_2O, 25% CO_2 and 75% H_2O, 100% H_2O.

The solid conversion (X_{OXI}), from a non-stoichiometry factor of 0.35 of the reduced metal oxide state to fully oxidized state, CeO_2, was evaluated with a variation of the reactor volume and of the composition of the inlet gas. As can be followed from the oxidation kinetics discussion in the reaction kinetics section, due to the relatively faster kinetics of water splitting, a higher conversion is achieved at a similar reactor volume as opposed to CO_2 splitting. The reaction kinetics, resulting in slowing down of the reaction with its degree of advancement, would practically limit the complete oxidation of the reduced metal oxide even after sufficiently increasing the reactor volume. Therefore, as can be seen from the following Figure 11, with 5% excess flow with respect to the stoichiometry for pure water splitting, the maximum solid conversion achieved for a 5 m^3 reactor volume was 98%, while for a reactor volume of 4 m^3, the corresponding conversion was 97.5%. The selectivity of the splitting product would follow the same profile as the metal oxide conversion and hence not plotted separately. Nevertheless, the selectivity of hydrogen for water splitting for a 4 and 5 m^3 reactor volume was obtained as 93.2% and 93.6% respectively, indicating the necessity of trade-off for selecting the moving bed reactor volume.

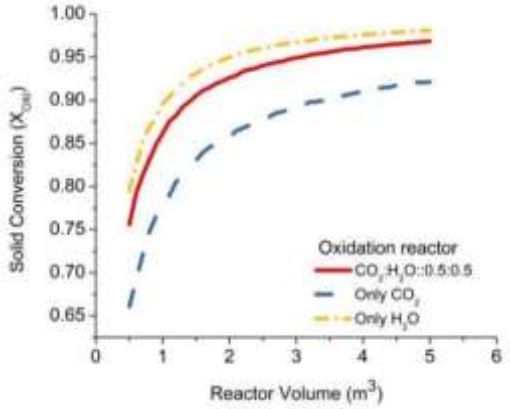

Figure 11. Impact of variation of the reactor volume on the solid conversion (X_{OXI}) in the oxidation reactor (OXI) with a variation of the inlet gas mixture composition, all other parameters, and molar flows being constant.

On the contrary, CO_2 splitting kinetics being slower than water splitting kinetics results in the solid conversion to be lower than that for water splitting, even though the variation of X_{OXI} with reactor volume follows a similar profile to that of water splitting. Corresponding to the 4 and 5 m^3 reactor, the solid conversion with CO_2 splitting was found to be 91% and 92% respectively, showing a higher relative increase in the yield with the same change in reactor volume as compared to water splitting. The corresponding CO selectivity is respectively 86.3% and 87.7%. All the mixtures of CO_2 and H_2O for co-splitting lie within the two limits whereby CO_2 provides the lower bound and H_2O the upper bound of the conversion. Nonetheless, the presence of water (steam) in the mixture enhances the reaction rate significantly, being not only more exothermic but also due to faster kinetics. Therefore, as can be followed from Figure 12, the co-splitting of an equimolar mixture of CO_2 and H_2O yields almost 96.2% solid conversion at a reactor volume of 4 m^3, a significant increase from stand-alone CO_2 splitting. The H_2/CO molar ratio was calculated as 1.06, showing similar selectivity of H_2 and CO, a major benefit of a moving bed reactor.

Indeed, a sensitivity to evaluate the solid conversion (X_{OXI}) with an increased flow of steam, together with an increased reactor volume was performed and the results are shown in Figure 12. The flow of steam was varied between 100 mol/s (stoichiometric) to 200 mol/s (stoichiometric excess 100%). As can be followed from Figure 12a, a moderate increase in the solid conversion of 0.4% can be seen up to 20% excess of flow for a reactor volume of 4 m^3, while the corresponding increase in yield is 0.6% and 0.2% for reactor volumes of 3 and 5 m^3 respectively. Nevertheless, beyond 20% of excess flow to the reactor, the relative increase in the metal oxide conversion becomes smaller, while the selectivity of the H_2 would drop proportionally because of the excess of reactant. Another disadvantage of sending much excess flow to the reactor, together with having a higher reactor operating volume can be concluded from Figure 12(b): where, a linear drop in the oxidized metal oxide outlet temperature is observed, with a drop of over 100°C for a 100% excess flow. Also, for more than 50% excess flow of steam and for a higher reactor volume, the outlet temperature is even lower, signifying a relative cooling of the oxidized metal oxide inside the reactor. Being a counter-current reactor, a higher reaction extent is seen for a larger reactor, which in turn lowers the oxidation reaction rate further. This

results in minimal reaction and hence a lower exothermicity of the reaction and a lower temperature of the outlet solid product is observed even though the conversion is higher. A higher temperature of the outlet metal oxide being always desired for decreasing the heat requirement for reduction as described in an earlier section this would require a reactor design optimization while performing the entire system in a redox cycle of thermal reduction of ceria with CO_2 and water splitting.

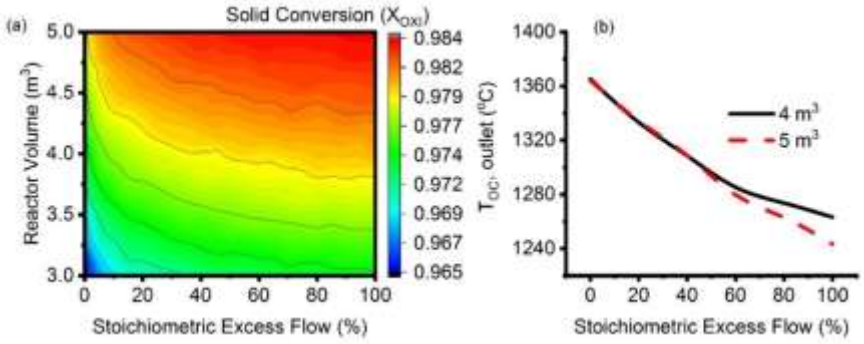

Figure 12. (a) Impact of variation of the reactor volume and the flow of steam (Stoichiometric excess) on the Solid Conversion (X_{OXI}) and (b) the variation of the metal oxide outlet temperature (Toc, outlet) with the flow of steam (stoichiometric excess) on the Solid Conversion (X_{OXI}) in the oxidation reactor (OXI) for water splitting for an inlet non-stoichiometry of 0.35, completely oxidized CeO_2 flow rate of 285.71 mol/s and pressure of 2 bar.

Based on the above discussion, a reactor volume of 4 m^3 was fixed to evaluate the variation of the solid conversion (X_{OXI}), and the metal oxide temperature (T_{OC}) along the length of the reactor for the five different gas compositions. As can be seen from Figure 13a, a similar reaction extent is noticed until around midway through the reactor length irrespective of the gas mixture composition. However, beyond that, with 50% or more fraction of water in the gas mixture, a considerable increase in the reaction extent occurs which results in the final solid conversion to be 97.6%, similar to that of only water splitting. However, below 50% water content in the inlet gas flow, the reaction rate drops, resulting in a slower reaction along the length of the reactor after midway through the reactor. The corresponding impact on the metal oxide temperature variation along the length of the reactor is evident as well. A higher exothermicity of water splitting results in proportionally higher metal temperatures attained within the reactor with an increased content of steam in the inlet gas mixture to the oxidation reactor. Indeed, both the reaction extent along the length of the reactor and the relative proportion of CO_2 and H_2O plays a crucial role in the metal oxide temperature within the reactor. For a faster water-splitting reaction, a maximum metal oxide temperature within the oxidation reactor of about 1460^{o}C is reached at about 80% of the reactor length, while a maximum reactor temperature of 1275^{o}C was achieved at similar stages along the reactor length for only CO_2 splitting. The drop in the metal oxide outlet temperature is due to a counterflow reactor configuration, whereby the cooler reactant gas being supplied results in cooling down of the metal oxide temperature by ~100^{o}C towards the end of the reactor length, as shown in Figure 13b. Also, at such later stages, due to the advanced condition of the oxidation, the reaction rate is much slower, resulting in lower exothermicity of the reaction. This lowering of the metal oxide temperature would result in the requirement of

higher heat in the reduction reactor as discussed earlier following Figure 6. One possible alternative can be a multi-entry reactor design whereby the gases can be fed in stages along the length of the reactor. This alternative was studied in brief and not reported in detail in the present work since the net outcome was found to decrease the metal oxide conversion in the OXI, even though the outlet metal oxide temperature from the OXI increased. Nevertheless, the benefit of working with water in splitting, even to lower extents over pure CO_2, can be emphasized through the following Figure 13. Even a presence of 50% of water in the CO_2/H_2O mixture ensures similar solid conversion to that of water splitting together with increasing the metal oxide outlet temperature from the OXI by almost a 100^{o}C from around 1150^{o}C to around 1300^{o}C for the same fixed reactor volume and fixed molar reactant gas flow.

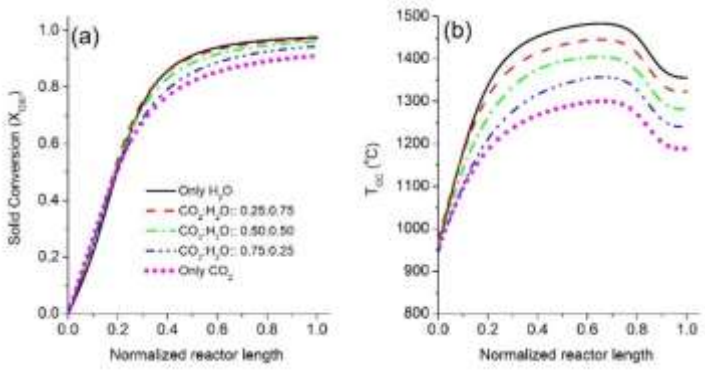

Figure 13. Variation of the Solid Conversion (X_{OXI}) (left) and metal oxide temperature (right) in the oxidation reactor with variable inlet gas mixture composition, at a constant oxidation reactor volume of 4 m^3, a constant non-stoichiometry factor of 0.35 and a constant inlet molar flow of reactant of 110 mol/s, with a fixed oxygen carrier and gas inlet temperature of 800^{o}C.

The impact of the variation of inlet temperatures of reactants and reduced metal oxide into the oxidation reactor (OXI) on the outlet temperature of oxidized metal and solid conversion have been investigated for a constant reactor volume (4 m^3) and fixed molar flows of both the solid and gaseous reactants. The two temperatures have been varied separately, maintaining the non-varying one at the constant value of 800^{o}C during the simulations. Figure 14a and b represent the impact of the gas inlet temperature on the outlet temperature of the oxidized metal oxide and the solid conversion, respectively. Irrespective of the variation of the metal oxide or gas inlet temperature, the impact of the relatively slower kinetics of the CO_2 compared to the water-splitting reaction is evident. A linear increase in the outlet metal oxide temperature of about 100^{o}C is noticed with an increase in the gas inlet temperature of 500^{o}C (from 500 to 1000^{o}C), which can be argued from the perspective of a counter-current flow in the reactor. No notable change in the relative solid conversion is however obtained, as can be followed from the previous discussions. A linear relation exists between the temperatures and the percentage of water in the inlet gas mixture. While a maximum $T_{OC,outlet}$ of 1398^{o}C was obtained for water splitting at a steam inlet temperature of 1000^{o}C, the lowest temperature of 1114^{o}C was found to occur for only CO_2 splitting for a CO_2 inlet temperature of 500^{o}C. Similar temperature profiles were observed for moving bed reactors by (Zahn et al., 2011).

Indeed, the metal oxide inlet temperature has also been varied and the results are reported by considering a constant gas inlet temperature of 800^{o}C, all other parameters being constant (Figure 14c and d). In fact, the results indicate this to be a better choice, since a significant increase in the metal oxide outlet temperature, as well as the overall

solid conversion is noticed. For a variation of 400°C of the reduced metal oxide inlet temperature a corresponding variation of 300°C in the outlet temperature of the metal oxide is noticed, irrespective of the composition of the inlet gas. It is noticed that for a metal oxide inlet temperature of 1000°C, the outlet temperature of the oxidized metal oxide increases to almost 1350°C, significantly improving the slower CO_2 splitting kinetics and hence the net metal oxide conversion (from 87% at 600°C to 92% at 1000°C of metal oxide inlet temperature). The relative impact of solid conversion decreases with the increase in the water content in the inlet gas mixture due to inherently faster water splitting kinetics and a more advanced oxidation condition (with the solid conversion of 97% for water splitting). Nonetheless, a high metal oxide outlet temperature of around 1500°C from the oxidation reactor can be seen, which would significantly reduce the heat requirement for reduction of ceria in the reduction reactor. However, whereby due to counter-current configuration, a very high metal oxide temperature within the reactor might occur. Thus, adequate reactor design optimization from multiple aspects is necessary to develop a moving bed oxidation reactor for CO_2 and H_2O splitting for a two-step chemical looping cycle with ceria. The results presented have further motivate in developing a closed loop reduction and oxidation moving bed reactor cycle and integrate into an oxyfuel power plant to investigate the efficiency of the solar thermochemical power generation, which is presented in a parallel study (Farooqui et al., n.d.).

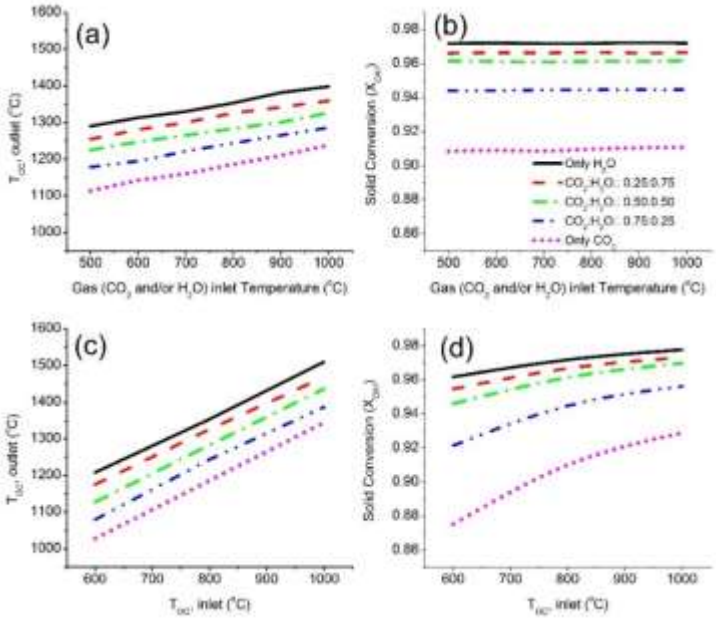

Figure 14. Variation of (a) metal oxide outlet temperature from the oxidation reactor and (b) solid conversion (X_{OXI}) in the oxidation reactor with variable gas inlet temperature; Variation of (c) metal oxide outlet temperature from the oxidation reactor and (d) solid conversion (X_{OXI}) with variable metal oxide inlet temperature ($T_{OC, inlet}$) in the oxidation reactor for a variable gas mixture composition at a constant oxidation reactor volume of 4 m^3, a constant inlet metal oxide non-stoichiometry factor of 0.35 and a constant molar flow of 105 mol/s of gas in the oxidation reactor.

5. Conclusion

In this paper, a comprehensive model was developed in ASPEN Plus® to simulate the chemical looping syngas fuel generation from water and carbon dioxide splitting in a dual moving bed reactor with redox cycling through ceria oxides. An extensive FORTRAN subroutine was developed to appropriately model the complexities of the reaction

kinetics. The kinetics subroutine was implemented in ASPEN Plus® moving bed reactor model. The entire set-up was evaluated considering an industrial scale application for the generation of 100 mol/s of syngas fuel. An isothermal reduction reactor and an adiabatic oxidation reactor model was developed and evaluated.

The sensitivity of the reduction reactor was studied by varying the temperature and pressure between 1200-1600^{o}C and 10^{-3} and 10^{-7} bar respectively. Close agreement with experimental data reported in literature was obtained for the reduction non-stoichiometry of ceria. A maximum reduction non-stoichiometry of 0.198 was obtained in the reduction reactor at 1600^{o}C and 10^{-7} bar pressure. The optimal residence time obtained was around 1.5 minutes, an increase in residence time will not yield any further benefit due to a faster backward reaction rate of recombination of the released oxygen in the reduction reactor.

For the oxidation reactor, system parametric sensitivity was studied considering maximum non-stoichiometry extent achievable for ceria of 0.35, as reported in the literature. The volume of the oxidation reactor to achieve 90% conversion of the reduced metal oxide was 8 times higher to that of the reduction reactor. The impact of the variation of the gas inlet temperature was found to be minimal, while an increase in the metal oxide inlet temperature would significantly increase the solid conversion and selectivity of the generated syngas fuel. A faster water splitting kinetics would result in not only a higher solid conversion and selectivity but also in a higher product outlet temperature due to higher exothermicity. Indeed, a relatively substantial increase in the yields from the oxidation reactor with 25% water in the gas mixture is noticed compared to working with pure CO_2. Nevertheless, similar selectivity from co-splitting of CO_2 and H_2O would allow generating an H_2/CO ratio similar to the input H_2O/CO_2 ratio. A large temperature variation along the length of the adiabatic oxidation reactor is also noticed, which would thus require further reaction design optimization of the moving bed oxidation reactor for CO_2 and/or H_2O splitting. This gives the motivation to further investigate the reactor model as a chemical looping syngas production unit as an add-on unit to the power plant and investigate the efficiency of the system which is presented in a parallel study (part II).

Acknowledgements

The research presented is performed within the framework of the SELECT+ 'Environomical Pathways for Sustainable Energy Systems' and funded with support from the Education, Audiovisual, and Culture Executive Agency (EACEA) of the European Commission. This publication reflects the views only of the author(s), and the Commission cannot be held responsible for any use, which may be made of the information contained therein. The financial support provided by InnoEnergy (E.I.T) and UPC is also highly appreciated. JL is a Serra Húnter Fellow and is grateful to the ICREA Academia program and grant GC 2017 SGR 128.

References

Abad, A., Adánez, J., García-Labiano, F., de Diego, L.F., Gayán, P., 2009. Modeling of the chemical-looping combustion of methane using a Cu-based oxygen carrier. Energy Procedia 1, 391–398. https://doi.org/10.1016/j.egypro.2009.01.053

Ackermann, S., Sauvin, L., Castiglioni, R., Rupp, J.L.M., Scheffe, J.R., Steinfeld, A., 2015. Kinetics of CO2 Reduction over Nonstoichiometric Ceria. J. Phys. Chem. C 119, 16452–16461. https://doi.org/10.1021/acs.jpcc.5b03464

Agrafiotis, C., Roeb, M., Sattler, C., 2015. A review on solar thermal syngas production via redox pair-based water/carbon dioxide splitting thermochemical cycles. Renew. Sustain. Energy Rev. 42, 254–285. https://doi.org/10.1016/j.rser.2014.09.039

Aresta, M., Dibenedetto, A., Angelini, A., 2013. The changing paradigm in CO2utilization. J. CO2 Util. 3–4, 65–73. https://doi.org/10.1016/j.jcou.2013.08.001

Arifin, D., 2013. Study of redox reactions to split water and carbon dioxide. University of Colorado.

Arifin, D., Weimer, A.W., 2018. Kinetics and mechanism of solar-thermochemical H2and CO production by oxidation of reduced CeO2. Sol. Energy 160, 178–185. https://doi.org/10.1016/j.solener.2017.11.075

ASPEN Plus® Model for Moving Bed Coal Gasifier-Aspen Technology tutorial, 2010.

Badillo-Hernandez, U., Alvarez-Icaza, L., Alvarez, J., 2013. Model design of a class of moving-bed tubular gasification reactors. Chem. Eng. Sci. 101, 674–685. https://doi.org/10.1016/j.ces.2013.07.001

Benjamin, B.W., 1985. Great Plains ASPEN Model Development: Gasifier Model. Final Topical Report. Sci. Des. Co., Inc., New York 180.

Brendelberger, S., Vieten, J., Vidyasagar, M.J., Roeb, M., Sattler, C., 2018. Demonstration of thermochemical oxygen pumping for atmosphere control in reduction reactions. Sol. Energy 170, 273–279. https://doi.org/10.1016/j.solener.2018.05.063

Brendelberger, S., von Storch, H., Bulfin, B., Sattler, C., 2017. Vacuum pumping options for application in solar thermochemical redox cycles – Assessment of mechanical-, jet- and thermochemical pumping systems. Sol. Energy 141, 91–102. https://doi.org/10.1016/j.solener.2016.11.023

Bulfin, B., 2015. Cerium dioxide redox cycle for fuel production. Trinity College, Dublin.

Bulfin, B., Lowe, A.J., Keogh, K.A., Murphy, B.E., Lübben, O., Krasnikov, S.A., Shvets, I. V., 2013. Analytical Model of CeO 2 Oxidation and Reduction. J. Phys. Chem. C 117, 24129–24137. https://doi.org/10.1021/jp406578z

Bulfin, B., Vieten, J., Agrafiotis, C., Roeb, M., Sattler, C., 2017. Applications and limitations of two step metal oxide thermochemical redox cycles; A review. J. Mater. Chem. A 5, 18951–18966. https://doi.org/10.1039/c7ta05025a

Chen, L., Yang, X., Li, G., Wen, C., Li, X., Snape, C., 2017. An Improved Form of Shrinking Core Model for Prediction of the Conversion during Reduction Process in Chemical Looping Combustion. Energy and Fuels 31, 1993–2006. https://doi.org/10.1021/acs.energyfuels.6b03036

Chueh, W.C., Haile, S.M., 2010. A thermochemical study of ceria: Exploiting an old material for new modes of energy conversion and CO2 mitigation. Philos. Trans. R. Soc. A Math. Phys. Eng. Sci. 368, 3269–3294. https://doi.org/10.1098/rsta.2010.0114

CO2 Capture Project (CCP), 2015. CCS Technology Development and Demonstration Results.

Cuéllar-Franca, R.M., Azapagic, A., 2015. Carbon capture, storage and utilisation technologies: A critical analysis and comparison of their life cycle environmental impacts. J. CO2 Util. 9, 82–102. https://doi.org/10.1016/j.jcou.2014.12.001

Davenport, T.C., Kemei, M., Ignatowich, M.J., Haile, S.M., 2017. Interplay of material thermodynamics and surface reaction rate on the kinetics of thermochemical hydrogen production. Int. J. Hydrogen Energy 42, 16932–16945. https://doi.org/10.1016/j.ijhydene.2017.05.184

Davenport, T.C., Yang, C.K., Kucharczyk, C.J., Ignatowich, M.J., Haile, S.M., 2016. Implications of Exceptional Material Kinetics on Thermochemical Fuel Production Rates. Energy Technol. 4. https://doi.org/10.1002/ente.201500506

Dawicke, J.W., Blumenthal, R.N., 1986. Oxygen association pressure measurements on nonstoichiometric cerium dioxide. J. Electrochem. Soc. 133, 904–909. https://doi.org/10.1149/1.2108760

Ehrhart, B.D., Muhich, C.L., Al-Shankiti, I., Weimer, A.W., 2016. System efficiency for two-step metal oxide solar thermochemical hydrogen production – Part 3: Various methods for achieving low oxygen partial pressures in the reduction reaction. Int. J. Hydrogen Energy 41, 19904–19914. https://doi.org/10.1016/j.ijhydene.2016.07.106

Ermanoski, I., 2014. Cascading pressure thermal reduction for efficient solar fuel production. Int. J.

Hydrogen Energy 39, 13114–13117. https://doi.org/10.1016/j.ijhydene.2014.06.143
Ermanoski, I., Siegel, N., Stechel, E., 2013a. A New Reactor Concept for Efficient Solar-Thermochemical Fuel Production. J. Sol. Energy Eng. 135, 31002. https://doi.org/10.1115/1.4023356
Ermanoski, I., Siegel, N.P., Stechel, E.B., 2013b. A New Reactor Concept for Efficient Solar-Thermochemical Fuel Production. J. Sol. Energy Eng. 135, 031002. https://doi.org/10.1115/1.4023356
Fan, D.L.-S., 2017. Chemical Looping Partial Oxidation: Gasification, Reforming, and Chemical Syntheses. Cambridge University Press.
Fan, J., Zhu, L., Jiang, P., Li, L., Liu, H., 2016. Comparative exergy analysis of chemical looping combustion thermally coupled and conventional steam methane reforming for hydrogen production. J. Clean. Prod. 131, 247–258. https://doi.org/10.1016/j.jclepro.2016.05.040
Farooqui, A., Bose, A., Ferrero, D., Lorca, J., Santarelli, M., n.d. Simulation of two-step redox recycling of non-stoichiometric ceria with thermochemical dissociation of CO2/H2O in moving bed reactors - Part II: Techno-economic analysis and integration with 100 MW oxyfuel power plant with carbon capture. Chem. Eng. Sci.
Farooqui, A.E., Pica, A.M., Marocco, P., Ferrero, D., Lanzini, A., Fiorilli, S., Llorca, J., Santarelli, M., 2018. Assessment of kinetic model for ceria oxidation for chemical-looping CO2 dissociation. Chem. Eng. J. 346, 171–181. https://doi.org/10.1016/j.cej.2018.04.041
He, C., Feng, X., Hoong, K., 2013. Process modeling and thermodynamic analysis of Lurgi fixed-bed coal gasifier in an SNG plant. Appl. Energy 111, 742–757. https://doi.org/10.1016/j.apenergy.2013.05.045
Ishida, T., Gokon, N., Hatamachi, T., Kodama, T., 2013. Kinetics of thermal reduction step of thermochemical two-step water splitting using CeO2 particles: Master-plot method for analyzing non-isothermal experiments. Energy Procedia 49, 1970–1979. https://doi.org/10.1016/j.egypro.2014.03.209
Ivan Ermanoski, 2013. Moving bed reactor for solar thermochemical fuel production. US 8.420,032 B1.
Ji, H. Il, Davenport, T.C., Gopal, C.B., Haile, S.M., 2016. Extreme high temperature redox kinetics in ceria: Exploration of the transition from gas-phase to material-kinetic limitations. Phys. Chem. Chem. Phys. 18, 21554–21561. https://doi.org/10.1039/c6cp01935h
Ji, H. Il, Davenport, T.C., Ignatowich, M.J., Haile, S.M., 2017. Gas-phase vs. material-kinetic limits on the redox response of nonstoichiometric oxides. Phys. Chem. Chem. Phys. 19, 7420–7430. https://doi.org/10.1039/c7cp00449d
Levenspiel, O., 1999a. Chemical reaction engineering, Ind. Eng. Chem. Res. https://doi.org/10.1021/ie990488g
Levenspiel, O., 1999b. Chapter 25. Fluid-Particle Reactions: Kinetics, in: Chemical Reaction Engineering. pp. 566–586.
Meylan, F.D., Moreau, V., Erkman, S., 2015. CO 2 utilization in the perspective of industrial ecology , an overview. Biochem. Pharmacol. 12, 101–108. https://doi.org/10.1016/j.jcou.2015.05.003
Muhich, C.L., Ehrhart, B.D., Al-Shankiti, I., Ward, B.J., Musgrave, C.B., Weimer, A.W., 2016. A review and perspective of efficient hydrogen generation via solar thermal water splitting. Wiley Interdiscip. Rev. Energy Environ. 5, 261–287. https://doi.org/10.1002/wene.174
Panlener, M.A., Blumenthal, R.N., Garnier, J.E., 1993. A thermodynamic and electrical conductivity study of nonstoichiometric cerium dioxide. Solid State Ionics 60, 279–298. https://doi.org/10.1016/0167-2738(93)90006-O
Roeb, M., Neises, M., Monnerie, N., Call, F., Simon, H., Sattler, C., Schmcker, M., Pitz-Paal, R., 2012. Materials-related aspects of thermochemical water and carbon dioxide splitting: A review. Materials (Basel). 5, 2015–2054. https://doi.org/10.3390/ma5112015
Scheffe, J.R., Steinfeld, A., 2014. Oxygen exchange materials for solar thermochemical splitting of H2O and CO2: A review. Mater. Today 17, 341–348. https://doi.org/10.1016/j.mattod.2014.04.025
Scheffe, J.R., Welte, M., Steinfeld, A., 2014. Thermal Reduction of Ceria within an Aerosol Reactor for H_2O and CO_2 Splitting. Ind. Eng. Chem. Res. 53, 2175–2182. https://doi.org/10.1021/ie402620k
Steinfeld, A., 2005. Solar thermochemical production of hydrogen - A review. Sol. Energy 78, 603–615. https://doi.org/10.1016/j.solener.2003.12.012

Tong, A., Zeng, L., Kathe, M. V, Sridhar, D., Fan, L., 2013. Application of the Moving-Bed Chemical Looping Process for High Methane Conversion. Energy & Fuels 27, 4119–4128. https://doi.org/10.1021/ef3020475

Tou, M., Michalsky, R., Steinfeld, A., 2017. Solar-Driven Thermochemical Splitting of CO2and In Situ Separation of CO and O2across a Ceria Redox Membrane Reactor. Joule 1, 146–154. https://doi.org/10.1016/j.joule.2017.07.015

Viebahn, P., Vallentin, D., Höller, S., 2015. Prospects of carbon capture and storage (CCS) in China's power sector - An integrated assessment. Appl. Energy 157, 229–244. https://doi.org/10.1016/j.apenergy.2015.07.023

Wheeler, V.M., Zapata, J., Kreider, P., Lipinski, W., 2018. Effect of non-stoichiometry on optical, radiative, and thermal characteristics of ceria undergoing reduction. Opt. Express 26, 1238–1243. https://doi.org/10.1364/oe-26-10-A360

Yadav, D., Banerjee, R., 2016. A review of solar thermochemical processes. Renew. Sustain. Energy Rev. 54, 497–532. https://doi.org/10.1016/j.rser.2015.10.026

Zahn, V.M., Yi, C.U., Seidel-Morgenstern, A., 2011. Analysis and demonstration of a control concept for a heat integrated simulated moving bed reactor. Chem. Eng. Sci. 66, 4901–4912. https://doi.org/10.1016/j.ces.2011.06.055

Zhao, Z., Uddi, M., Tsvetkov, N., Yildiz, B., Ghoniem, A.F., 2016. Redox Kinetics Study of Fuel Reduced Ceria for Chemical-Looping Water Splitting. J. Phys. Chem. C 120, 16271–16289. https://doi.org/10.1021/acs.jpcc.6b01847

Zimmermann, A.W., Schom, R., 2017. Assessing Early-Stage CO 2 utilization Technologies — Comparing Apples and Oranges ? 850–860. https://doi.org/10.1002/ente.201600805